Publ. Astron. Soc. Japan (2014) 00(0), 1–15
doi: 10.1093/pasj/xxx000

OISTER Optical and Near-Infrared Monitoring Observations of a Peculiar Radio-Loud Active Galactic Nucleus SDSS J110006.07+442144.3

Tomoki Morokuma[1], Masaomi Tanaka[2], Yasuyuki T. Tanaka[3], Ryosuke Itoh[4,5], Nozomu Tominaga[6,7], Poshak Gandhi[8], Elena Pian[9,10], Paolo Mazzali[11,12], Kouji Ohta[13], Emiko Matsumoto[6], Takumi Shibata[6], Hinako Akimoto[14], Hiroshi Akitaya[15,3], Gamal B. Ali[16], Tsutomu Aoki[17], Mamoru Doi[1,18], Nana Ebisuda[5], Ahmed Essam[16], Kenta Fujisawa[19], Hideo Fukushima[2], Shuhei Goda[20], Yuya Gouda[20], Hidekazu Hanayama[21], Yasuhito Hashiba[1,36], Osamu Hashimoto[22], Kenzo Hayashida[23], Yuichiro Hiratsuka[24], Satoshi Honda[14], Masataka Imai[20], Kanichiro Inoue[23], Michiko Ishibashi[24], Ikuru Iwata[25], Hideyuki Izumiura[26], Yuka Kanda[5], Miho Kawabata[5], Kenji Kawaguchi[5], Nobuyuki Kawai[4], Mitsuru Kokubo[27,36,1], Daisuke Kuroda[26], Hiroyuki Maehara[26,17], Hiroyuki Mito[17], Kazuma Mitsuda[1], Ryota Miyagawa[24], Takeshi Miyaji[21], Yusuke Miyamoto[28,15], Kumiko Morihana[14], Yuki Moritani[7,3], Kana Morokuma-Matsui[29,2], Kotone Murakami[23], Katsuhiro L. Murata[30], Takahiro Nagayama[23], Kazuki Nakamura[24], Tatsuya Nakaoka[5], Kotaro Niinuma[31], Takafumi Nishimori[23], Daisaku Nogami[13], Yumiko Oasa[24,32], Tatsunori Oda[24], Tomohito Ohshima[14], Yoshihiko Saito[4], Shuichiro Sakata[23], Shigeyuki Sako[1], Yuki Sarugaku[17], Satoko Sawada-Satoh[15], Genta Seino[24], Kazuo Sorai[33], Takao Soyano[17], Francesco Taddia[34], Jun Takahashi[14], Yuhei Takagi[2,14], Katsutoshi Takaki[5], Koji Takata[5], Ken'ichi Tarusawa[17], Makoto Uemura[3], Takahiro Ui[5], Riku Urago[23], Kazutoshi Ushioda[24], Jun-ichi Watanabe[2], Makoto Watanabe[35,20], Satoshi Yamashita[23], Kenshi Yanagisawa[26], Yoshinori Yonekura[15] and Michitoshi Yoshida[25,3]

[1]Institute of Astronomy, Graduate School of Science, University of Tokyo, 2-21-1, Osawa, Mitaka, Tokyo 181-0015, Japan
[2]National Astronomical Observatory of Japan, National Institutes of Natural Sciences, 2-21-1, Osawa, Mitaka, Tokyo 181-8588, Japan
[3]Hiroshima Astrophysical Science Center, Hiroshima University, Higashi-Hiroshima, Hiroshima 739-8526, Japan
[4]Department of Physics, Tokyo Institute of Technology, 2-12-1 Ookayama, Meguro-ku, Tokyo 152-8551, Japan
[5]Department of Physical Science, Hiroshima University, Kagamiyama 1-3-1, Higashi-Hiroshima 739-8526, Japan
[6]Department of Physics, Faculty of Science and Engineering, Konan University, 8-9-1 Okamoto, Kobe, Hyogo 658-8501, Japan

[7]Kavli Institute for the Physics and Mathematics of the Universe (WPI), The University of Tokyo, 5-1-5 Kashiwanoha, Kashiwa, Chiba 277-8583, Japan
[8]Department of Physics and Astronomy, University of Southampton, Highfield, Southampton SO17 1BJ, UK
[9]Institute of Space Astrophysics and Cosmic Physics, via P. Gobetti 101, I-40129 Bologna, Italy
[10]Scuola Normale Superiore, Piazza dei Cavalieri 7, I-56126 Pisa, Italy
[11]Astrophysics Research Institute, Liverpool John Moores University, IC2, Liverpool Science Park, 146 Brownlow Hill, Liverpool L3 5RF, UK
[12]Max-Planck-Institut fr Astrophysik, Karl-Schwarzschild-Str. 1, D-85748 Garching, Germany
[13]Department of Astronomy, Graduate School of Science, Kyoto University, Sakyo-ku, Kyoto 606-8502, Japan
[14]Nishi-Harima Astronomical Observatory, Center for Astronomy, University of Hyogo, 407-2 Nishigaichi, Sayo, Hyogo 679-5313, Japan
[15]Center for Astronomy, Ibaraki University, 2-1-1 Bunkyo, Mito, Ibaraki 310-8512, Japan
[16]National Research Institute of Astronomy and Geophysics, 11421 Helwn, Cairo, Egypt
[17]Kiso Observatory, Institute of Astronomy, School of Science, The University of Tokyo 10762-30, Mitake, Kiso-machi, Kiso-gun, Nagano 397-0101, Japan
[18]Research Center for the Early Universe, Graduate School of Science, The University of Tokyo, 7-3-1 Hongo, Bunkyo-ku, Tokyo 113-0033, Japan
[19]The Research Institute of Time Studies, Yamaguchi University, 1677-1 Yoshida, Yamaguchi, Yamaguchi 753-8511, Japan
[20]Department of Cosmosciences, Hokkaido University, Kita 10 Nishi 8, Kita-ku, Sapporo, Hokkaido 060-0810, Japan
[21]Ishigakijima Astronomical Observatory, National Astronomical Observatory of Japan, National Institutes of Natural Sciences, Ishigaki, Okinawa 907-0024, Japan
[22]Gunma Astronomical Observatory, Takayama, Gunma 377-0702, Japan
[23]Graduate School of Science and Engineering, Kagoshima University, 1-21-35 Korimoto, Kagoshima 890-0065, Japan
[24]Faculty of Education, Saitama University, 255 Shimo-Okubo, Sakura, Saitama, 338-8570, Japan
[25]Subaru Telescope, National Astronomical Observatory of Japan, National Institutes of Natural Sciences, 650 North A'ohoku Place, Hilo, HI 96720, USA
[26]Okayama Astrophysical Observatory, National Astronomical Observatory of Japan, National Institutes of Natural Sciences, 3037-5 Honjo, Kamogata, Asakuchi, Okayama 719-0232, Japan
[27]Astronomical Institute, Tohoku University, Aramaki, Aoba-ku, Sendai, 980-8578, Japan
[28]Nobeyama Radio Observatory, National Astronomical Observatory of Japan, National Institutes of Natural Sciences, 462-2 Nobeyama, Minamimaki, Nagano 384-1305, Japan
[29]The Institute of Space and Astronautical Science, Japan Aerospace Exploration Agency, 3-1-1 Yoshinodai, Chuo-ku, Sagamihara, Kanagawa 252-5210, Japan
[30]Department of Astrophysics, Nagoya University, Chikusa-ku, Nagoya 464-8602, Japan
[31]Graduate School of Sciences and Technology for Innovation, Yamaguchi University, 1677-1 Yoshida, Yamaguchi, Yamaguchi 753-8512, Japan
[32]Department of Physics, Graduate School of Science and Engineering, Saitama University, 255 Shimo-Okubo, Sakura, Saitama, 338-8570, Japan
[33]Department of Physics, Faculty of Science, Hokkaido University, Kita-ku, Sapporo 060-0810, Japan
[34]The Oskar Klein Centre, Department of Astronomy, Stockholm University, AlbaNova, SE-10691 Stockholm, Sweden
[35]Department of Applied Physics, Okayama University of Science, 1-1 Ridai-cho, Kita-ku,

Okayama, Okayama 700-0005, Japan
[36]JSPS Fellow

*E-mail: tmorokuma@ioa.s.u-tokyo.ac.jp

Received ; Accepted

Abstract

We present monitoring campaign observations at optical and near-infrared (NIR) wavelengths for a radio-loud active galactic nucleus (AGN) at $z = 0.840$, SDSS J110006.07+442144.3 (hereafter, J1100+4421), which was identified during a flare phase in late February, 2014. The campaigns consist of three intensive observing runs from the discovery to March, 2015, mostly within the scheme of the OISTER collaboration. Optical-NIR light curves and simultaneous spectral energy distributions (SEDs) are obtained. Our measurements show the strongest brightening in March, 2015. We found that the optical-NIR SEDs of J1100+4421 show an almost steady shape despite the large and rapid intranight variability. This constant SED shape is confirmed to extend to ~ 5 μm in the observed frame using the archival WISE data. Given the lack of absorption lines and the steep power-law spectrum of $\alpha_\nu \sim -1.4$, where $f_\nu \propto \nu^{\alpha_\nu}$, synchrotron radiation by a relativistic jet with no or small contributions from the host galaxy and the accretion disk seems most plausible as an optical-NIR emission mechanism. The steep optical-NIR spectral shape and the large amplitude of variability are consistent with this object being a low $\nu_{\rm peak}$ jet-dominated AGN. In addition, sub-arcsec resolution optical imaging data taken with Subaru Hyper Suprime-Cam does not show a clear extended component and the spatial scales are significantly smaller than the large extensions detected at radio wavelengths. The optical spectrum of a possible faint companion galaxy does not show any emission lines at the same redshift and hence a merging hypothesis for this AGN-related activity is not supported by our observations.

Key words: relativistic processes — accretion, accretion disks — quasars: supermassive black holes — quasars: individual (SDSS J110006.07+442144.3)

1 Introduction

Since the detection of γ-ray emission from narrow-line Seyfert 1 galaxies (NLS1s; Abdo et al. 2009a), which are one of the low-mass populations of active galactic nuclei (AGN), the nature of systems with relativistic jets but lower masses than blazars and radio galaxies has attracted much attention from researchers in fields such as AGN, relativistic phenomena, and galaxies. These γ-ray-loud NLS1s have in general smaller black hole (BH) masses of $M_{\rm BH} \sim 10^{6-8}$ M$_\odot$ (Abdo et al. 2009a) for the first four γ-ray-loud NLS1s than blazars with larger BHs of $< M_{\rm BH} >= 2.8 \times 10^8$ M$_\odot$(Pian et al. 2005), even though such strong jet activities are thought to be generally associated with massive systems. Multi-wavelength observational studies on these populations, including γ-ray (Abdo et al. 2009b), X-ray, high-resolution radio VLBI (Doi et al. 2012), provide clues to the relationship between the central engines and jet formation mechanisms, AGN triggering mechanisms, and possibly BH growth (from lower to higher masses in quasars and elliptical galaxies). However, these observational studies have been done for a limited number of objects while statistical studies on NLS1s were recently done in several papers (e.g., Foschini et al. 2015).

The rapid optical flare of the extragalactic object SDSS J110006.07+442144.3 (J1100+4421, hereafter) was initially recognized on February 23, 2014 (Tanaka et al. 2014), during the 1-hour-cadence Kiso Supernova Survey (KISS; Morokuma et al. 2014), which utilizes the 105-cm Kiso Schmidt telescope and its optical wide-field imager, the Kiso Wide Field Camera (KWFC; Sako et al. 2012). Quick imaging and spectroscopic follow-up observations with the Faint Object Camera and Spectrograph (FOCAS; Kashikawa et al. 2002) on the Subaru 8.2-m telescope right after the flare detection indicated that the object was a narrow-line AGN at $z = 0.840$ with a small BH mass of $M_{\rm BH} = 1.0 - 1.5 \times 10^7$ M$_\odot$ and a sub-Eddington ratio of $L_{\rm bol}/L_{\rm Edd} \sim 0.3$ (Tanaka et al. 2014). By combining these optical data with archival radio, infrared (WISE), γ-ray (Fermi) data and X-ray data taken via a ToO observation with X-ray Telescope (XRT) on board the Swift satellite, Tanaka et al. (2014) revealed the similarity of this object's SED to those of the radio/γ-ray-loud NLS1s, although the large [O III]/Hβ

flux ratio does not satisfy the general criteria for NLS1s. Flux ratio between the [O III] emission lines and radio emission is also consistent with those of radio-loud NLS1s (Berton et al. 2016).

To examine the origins of the emission mechanisms and variability of J1100+4421, we carried out intensive monitoring observations under the auspices of the global telescope network known as Optical and Infrared Synergetic Telescopes for Education and Research (OISTER[1]; Sekiguchi et al. 2017). OISTER is one of the best observational organizations to achieve continuous, long-term monitoring observations in optical and near-infrared wavelengths for relatively bright objects because of its multi-site observing facilities.

In this paper, we describe our imaging monitoring observations and additional spectroscopic observations in Section 2. Results of the data analyses for the observational data are shown in Section 3. The implications of the observational results on the emission mechanisms and the host galaxy and environmental properties are described in Section 4. We summarize the content of the paper in Section 5.

Cosmological parameters used in this paper are $\Omega_M = 0.3, \Omega_\Lambda = 0.7, H_0 = 70$ km s^{-1} Mpc^{-1}. All the observing times are specified in UT. All magnitudes in optical and near-infrared wavelengths are measured in AB system unless otherwise noted. Galactic extinctions (Schlafly & Finkbeiner 2011), $A_u = 0.055, A_g = 0.043, A_r = 0.029, A_i = 0.022, A_z = 0.016, A_J = 0.009, A_H = 0.006$, and $A_{K_s} = 0.004$ mag, are not corrected for the photometric values in Table 2 or the spectra shown in Figure 3 while they are corrected in calculating the SEDs and fitted power-law indices. Note that power-law indices of the spectral energy distribution (SED), α_ν, measured in this paper are defined as $f_\nu \propto \nu^{\alpha_\nu}$.

2 Monitoring Campaign Observations and Data Reduction

2.1 Optical and Near-Infrared Imaging

2.1.1 Observations

We used 10 telescopes and 12 instruments in Japan among the OISTER collaboration to take most of the imaging data presented in this paper. Instruments used (from east to west in Japan) are a visible Multi-Spectral Imager (MSI; Watanabe et al. 2012) on the 1.6-m Pirka telescope, the FLI Micro Line Deep Depletion CCD camera on the 0.55-m Saitama university Common-use Research for Astronomy (SaCRA) telescope, MITSuME (Kotani et al. 2005; Yatsu et al. 2007; Shimokawabe et al. 2008) on the 0.5-m Akeno telescope, KWFC (Sako et al. 2012) on the 1.05-m Kiso Schmidt telescope, Line Imager and Slit Spectrograph (LISS; Hashiba et al. 2014) and Nishi-Harima Infrared Camera (NIC) on the 2.0-m Nayuta telescope, Kyoto Okayama Optical Low-dispersion Spectrograph (KOOLS; Yoshida 2005) and ISLE (Yanagisawa et al. 2008) on the 1.88-m Okayama Astrophysical Observatory (OAO) telescope, MITSuME on the 0.5-m OAO telescope (Kotani et al. 2005; Yanagisawa et al. 2010), Hiroshima Optical and Near-InfraRed camera (HONIR; Akitaya et al. 2014; Sakimoto et al. 2012) on the 1.5-m Kanata telescope, a near-infrared camera on the 1.0-m Kagoshima telescope, and MITSuME on the 1.05-m Murikabushi telescope.

In addition, we also took B-band images with the 1.88-m telescope at the Kottamia Astronomical Observatory (KAO) in Egypt on Feb. 9, 2015 and imaging data with Hyper Suprime-Cam (HSC; Miyazaki et al. 2012) on the Subaru 8.2-m telescope in Hawaii, in g-band on November 27, 2014 and May 24, 2015, and in z-band on Novermber 26, 2014, respectively. The plate scales and fields-of-view of these two instruments are 0.304 arcsec^{-1} pixel and 10 arcmin, and 0.168 arcsec^{-1} pixel and 1.5 degree in diameter of a circular shape field-of-view, respectively.

The observing epochs fall into three intensive campaigns: from February, 2014 to March, 2014, right after the discovery described in Tanaka et al. (2014), from October, 2014 to November, 2014, and in March 2015. In the second observing campaign, from Oct 2014 to Nov 2014, we obtained data at least once in multiple bands almost every night if the weather permitted. During the third observing epoch, optical imaging data with OAO188 KOOLS were taken 2-3 times per night over 4 continuous nights, at intervals of a few hours, if the weather permitted.

The instruments used in this campaign nicely cover a wide range of wavelengths from optical to NIR, from u-band to K_s-band as shown in Table 2.

2.1.2 Data Reduction

Basic data reduction for imaging data was done in a standard manner. Bias subtraction, overscan subtraction (if necessary), flat-fielding, sky subtraction, and astrometry procedures are done with a data reduction pipeline for each instrument. We combined all images taken within a night to create one stacked image per day, except for the discovery and quick follow-up data shown in Tanaka et al. (2014) and the OAO KOOLS optical data in March 2015. The HSC data was reduced using hscPipe version 3.8.5, which was developed based on the LSST pipeline (Ivezic et al. 2008; Axelrod et al. 2010).

For these reduced images, we performed forced photometry by fixing the coordinates of J1100+4421 and the reference stars (Table 1) into consistent locations, using the *Common-use Automatic Realtime Photometry* (CARP) pipeline (Saito et al. 2017), which has been developed to conduct photometry for images taken by the OISTER collaboration, The adopted aperture size was set to be three times the seeing FWHM in diameter.

[1] http://oister.oao.nao.ac.jp/

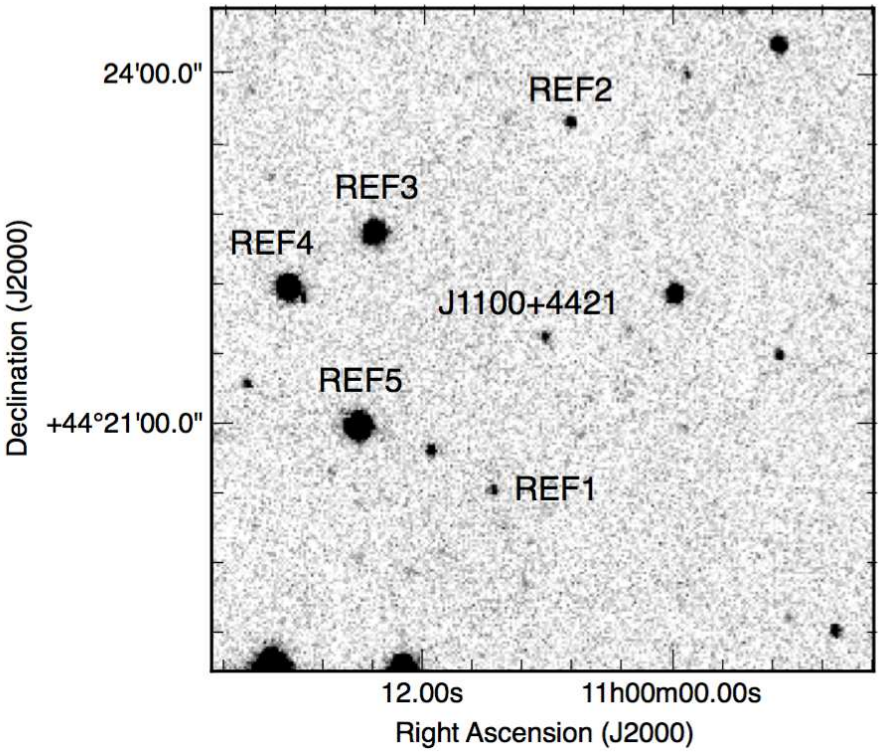

Fig. 1. The Kiso KWFC g-band image of the field at the discovery epoch. The central object in the figure is the target J1100+4421. The reference stars for the relative photometry are marked. North is up and east is left. The box size is 6 arcmin square.

For images with $< 3\sigma$ detections for J1100+4421, we set 3σ upper limits provided by the CARP pipeline.

According to the fields-of-view and filters of the images, different reference stars may be used in different images, although the same stars were used in a given filter as much as possible. Most of the data were calibrated via star #2 in optical and the star #3 in NIR. In the optical wavelengths, $ugriz$-band magnitudes of the reference stars are derived from SDSS Data Release 12 (DR12; Alam et al. 2015) and $BVRI$-band magnitudes are calculated from the SDSS magnitudes using the conversion equations shown in Jester et al. (2005). Magnitudes of the reference stars in NIR wavelengths are derived from the 2MASS database (Skrutskie et al. 2006) and converted to those in the AB system as follows: $J_{\rm AB} = J_{\rm Vega} + 0.94$, $H_{\rm AB} = H_{\rm Vega} + 1.38$, and $K_{s,{\rm AB}} = K_{s,{\rm Vega}} + 1.86$ (Tokunaga & Vacca 2005).

The reference stars #1, and #2 have nearby stars separated by 3.5 arcsec and 6.2 arcsec, respectively, which are at least 3.4 mag fainter in optical wavelengths than the reference stars. Most of our imaging data were taken under seeing of a few arcsec and these nearby stars contaminate the flux measurements of the reference stars. However, the fraction of flux contributed by these nearby stars is estimated to be typically a factor of ~ 0.02 by comparing the SDSS magnitudes of the stars and does not affect our conclusions.

In principle, using different reference stars for relative photometry could provide different magnitudes for the target. The spectral slopes of J1100+4421, as described in §3.3, are comparable to those of cool, red stars. We checked for possible systematic differences in relative photometry with different stars of different spectral slopes (colors) and confirmed that the differences of the resulting magnitudes are smaller than 10%, even if we use a blue star as a reference star. Therefore, we conclude that the choice of the reference stars does not affect our conclusions, which require only about 10% accuracy.

As shown in Section 4.3, there is a faint galaxy 2.7 arcsec away from the object, which also contaminates the flux of the object. The measured brightness ($g = 25.32$ mag, $z = 22.15$ mag) is roughly 10 times or more fainter than the object in most of the detected epochs although these factors depend on the brightness phase of the object. These are also small effects on our photometries and resultant discussion.

2.2 Optical Spectroscopy

2.2.1 Observations

In addition to the Subaru FOCAS spectra obtained in February, 2014 (Tanaka et al. 2014), we took a new long-slit spectrum of a 900-sec exposure using the grating R400 and the order-sort filter OG515 with the Gemini Multi-Object Spectrographs

Table 1. SDSS and 2MASS photometry of the References Stars.

Ref	RA	Dec	u	g	r	i	z	J	H	K_s
1	11:00:08.54	+44:20:25.95	23.81(0.68)	20.26(0.02)	18.80(0.01)	17.94(0.01)	17.51(0.01)	16.40(0.11)	15.69(0.12)	15.59(0.17)
2	11:00:04.87	+44:23:34.51	21.96(0.17)	19.67(0.01)	18.75(0.01)	18.39(0.01)	18.21(0.02)	-	-	-
3	11:00:14.17	+44:22:38.39	18.64(0.02)	16.15(0.00)	15.08(0.00)	14.66(0.00)	14.46(0.00)	13.36(0.02)	12.72(0.02)	12.60(0.02)
4	11:00:18.37	+44:22:09.50	17.65(0.01)	15.66(0.00)	14.97(0.00)	14.70(0.00)	14.60(0.00)	13.62(0.02)	13.15(0.02)	13.06(0.03)
5	11:00:14.97	+44:20:58.44	16.73(0.01)	14.93(0.00)	14.31(0.00)	14.59(0.00)	13.97(0.00)	13.01(0.02)	12.61(0.02)	12.49(0.02)

JHK magnitudes are shown in the Vega system, which are the raw values in the 2MASS catalog. Magnitude errors are shown in the parenthesis.

(GMOS; Hook et al. 2004) on the Gemini-North 8.1-m telescope on December 11, 2015. The resulting wavelength range is 5150-9400Å. The slit width was 1.0 arcsec and the spectral resolution was $R \sim 940$. The slit was aligned with J1100+4421 and a nearby galaxy located about 2.7 arcsec to the south-east. Although the sky was clear, it was windy and then the seeing was bad and variable from 1.1 arcsec to 3.2 arcsec during the night.

We note that atmospheric dispersion corrector (ADC) is not available for GMOS while an ADC is equipped with the Cassegrain focus and available for FOCAS on the Subaru telescope. The resultant slit loss is estimated in some cases and available on the Gemini website[2]. The position angle of the slit was 115.0 deg (east from north) and the parallactic angle was ~ -140 deg. Then, the difference of the angles was ~ 105 deg causing the differential slit loss of $\sim 20\%$ over the observed wavelength range. On the other hand, the standard star used for flux calibration, Feige 110, was observed at the parallactic angle on the same night.

2.2.2 Data Reduction

The GMOS spectrum was reduced with the Gemini IRAF package. The reduction procedure was basically equivalent to that done for the FOCAS spectra (Tanaka et al. 2014). Wavelength calibration was done using the CuAr lamp spectrum. The obtained GMOS spectrum and the FOCAS spectra on February 23, 2014 (Tanaka et al. 2014) are shown in Figure 3. Note that the GMOS spectrum was obtained without the ADC and the relative flux calibration is not correct at $\sim 20\%$ level.

3 Results

3.1 Light Curves

The obtained light curves (LCs) are shown in Figure 2 and summarized in Table 2. Deep observations in which the object is detected with a high significance are limited because of the faintness of the object for 1-2m-class telescopes. The object, when detected, was brighter than the SDSS magnitudes measured for the $ugriz$-band images taken in 2003; the SDSS magnitudes are the faintest among our data, although the depths of most of our images are shallower than the SDSS magnitudes.

As described in Section 2.1, the observing data mostly consist of three campaigns. We below summarize the brightness changes separately in each of these three observing epochs.

First, we briefly summarize the discovery with Kiso KWFC and 1-month follow-up observations after the discovery, which were described in detail in Tanaka et al. (2014). The object showed a rapid increase in brightness from non-detection ($g > 20 - 21$ mag) to 19.73 ± 0.13 mag on February 23, 2014. After that, the object quickly faded down to $21 - 22$ mag during the discovery night at Kiso and the next 24 hours at Mauna Kea, Hawaii. We monitored the object after this discovery over about 1 month with Kiso KWFC (g-band), Kottamia Observatory 1.88-m telescope (V-band), Akeno MITSuME (g, R_C, I_C-bands), OAO KOOLS (g-band), and Kanata HONIR (R_C, J-bands). The data sampling was sparse, but the object seemed to brighten a few times to a level similar to that of the discovery epoch. The peak magnitude in this observing epoch in blue optical bands was $V = 19.17 \pm 0.13$ mag and that in NIR was $K_s = 17.68 \pm 0.22$.

In the second observing campaign, we did not detect the object on most of the nights during bright moon phases, placing only weak upper limits on its brightness at those times. Compared to the first and third observing epochs, the object was fainter, reaching only to $R_C = 19.58 \pm 0.19$ mag and $K_s = 18.91 \pm 0.21$ even at its peak.

The object was at its brightest in this third observing epoch, up to 18.58 ± 0.11 mag in g-band (brighter than the discovery epoch by a factor of ~ 2.9 in flux units) and 18.07 ± 0.10 mag in R_C-band. In addition, the object was also the brightest in NIR, $K_s = 17.45 \pm 0.20$.

3.2 Variability Time Scale

Variability time scales, in general, provide useful information to constrain the size of an emitting region and the emission mechanism producing the variability. We adopt a doubling/halving time scale τ as an indicator of the variability,

$$F(t) = F_0(t) 2^{-(t-t_0)/\tau} \quad (1)$$

following equation (1) in Foschini et al. (2011). As done in Foschini et al. (2011) for flat-spectrum radio quasars at MeV energies, the time scale τ is calculated only for a combination

[2] http://www.gemini.edu/sciops/instruments/gmos/itc-sensitivity-and-overheads/atmospheric-differential-refraction

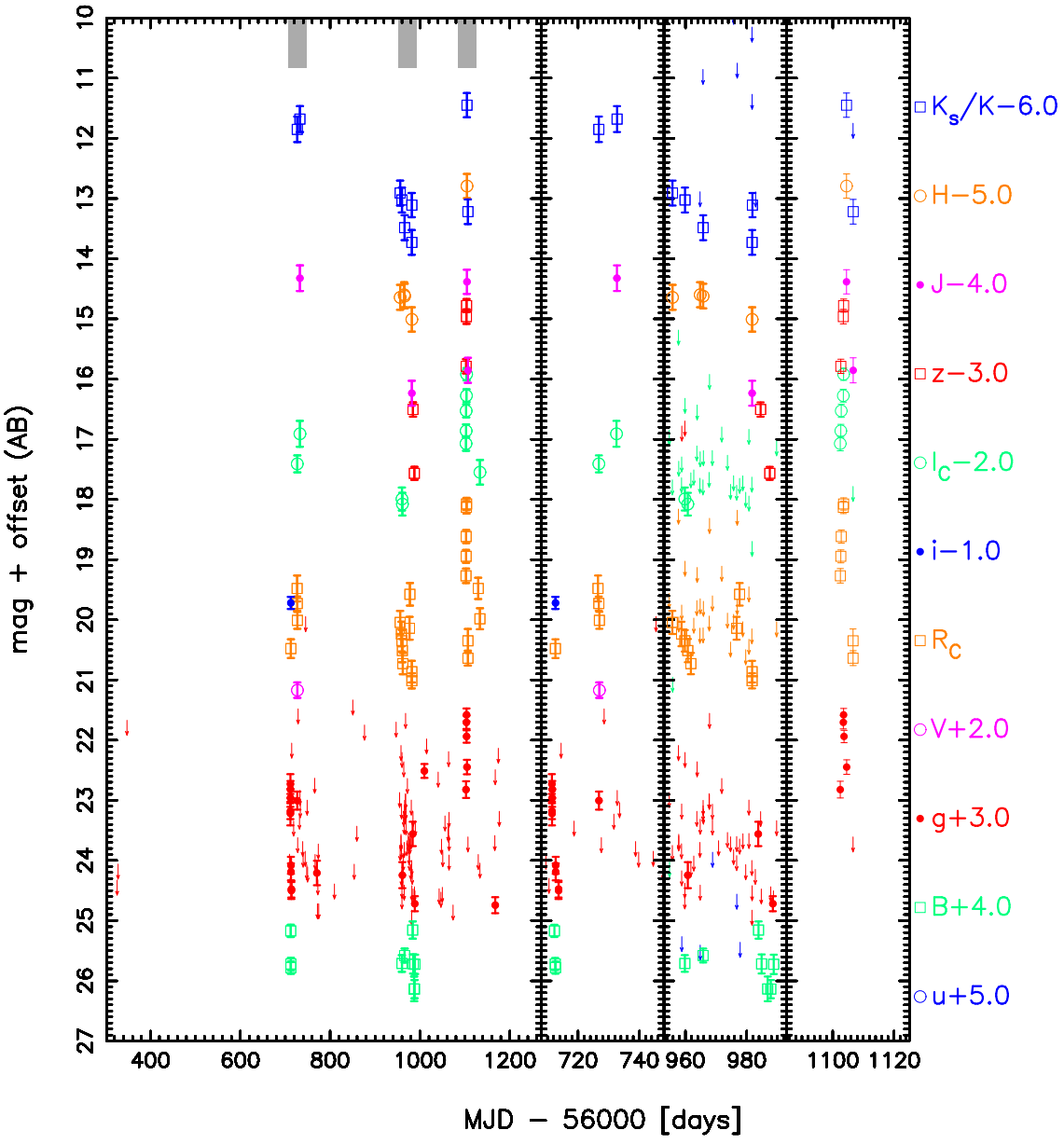

Fig. 2. Light curves of SDSS J110006.07+442144.3 in magnitude unit. u in blue, B in green, g in red, V in purple, R_C in orange, i in blue, I_C in green, z in red, J in purple, H in orange, and K_s and K in blue. *Left Panel*: Entire light curves of J1100+4421. Upper limits only in g-band are shown. Time ranges magnified in the right panels are shown in gray at the top of the panel. *Three Right Panels*: Light curves of J1100+4421 focused around the discovery epoch, the Oct-Nov 2014 campaign observing run, and the bright epoch in March 2015, respectively. Upper limits in all the filters are shown. Galactic extinctions are not corrected.

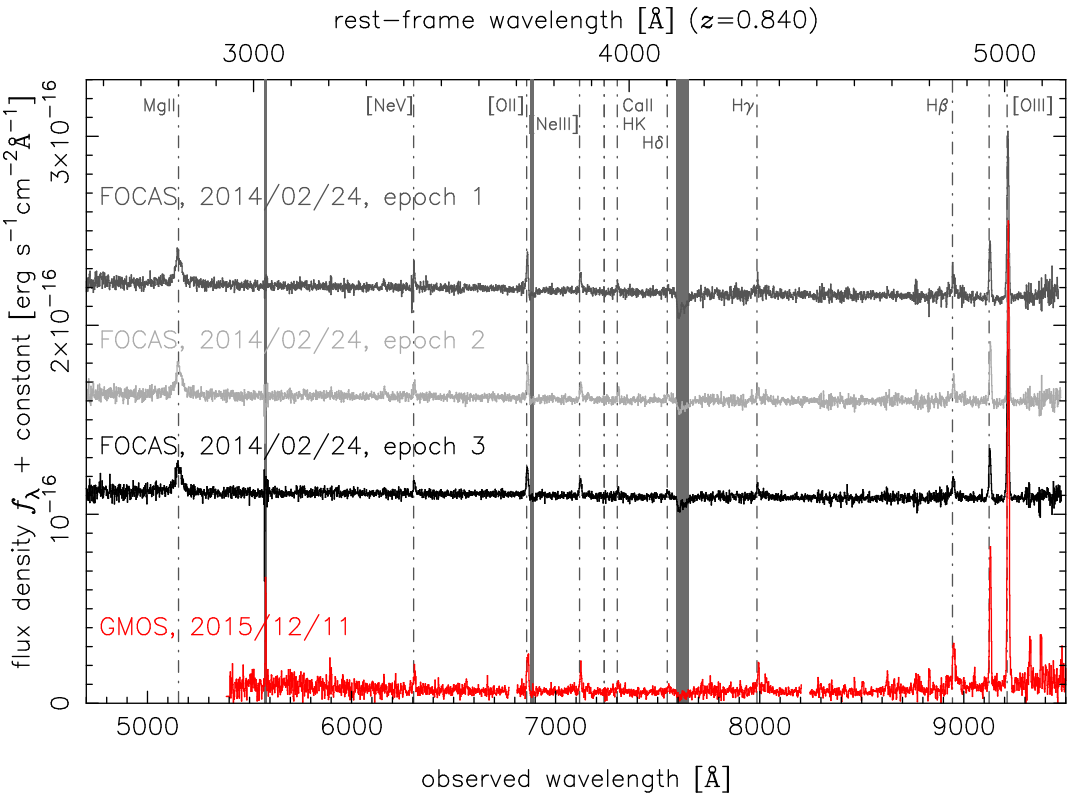

Fig. 3. A comparison of optical spectra taken with Subaru FOCAS on February 24, 2014 (already shown in Tanaka et al. 2014) and Gemini-N GMOS newly obtained on December 11, 2015. The GMOS spectrum is separated into three wavelength ranges because the gaps between the adjacent GMOS CCDs. Emission and absorption lines which could originate from an AGN and a galaxy are indicated in dot-dashed lines. Note that all the indicated lines are not detected. Strong telluric absorptions (O_2 A-band and B-band) and a strong OH airglow emission around 5,577Å causing bad sky subtraction are shaded in dark gray. Galactic extinctions are not corrected.

of the measurements which show significant ($> 3\sigma$) variability.

The shortest halving time scale τ in the observed frame obtained in our study is $\tau = 0.38 \pm 0.18$ days ($\sim 9.2 \pm 4.5$ hours). This is derived from the data taken on MJD 56712, on the night of our quick follow-up observations with Subaru FOCAS. Because of our limited time sampling and depths, the real typical halving time scale could be shorter than the obtained value. Compared with previous works on variability time scales of blazars in UV, optical, and NIR wavelength regions (Urry et al. 1997), in which optical flares over time scales from minutes to days are detected, the time scale of J1100+4421 is longer than most of those values, even though the BH mass of our object is smaller than those in blazars by a few orders of magnitude. If we assume a Doppler boosting factor of $\delta = 10$ for J1100+4421, similar to that of blazars (Fan et al. 2013), the size of the optical-NIR emission region R is evaluated (Zhang et al. 2012) as $R < c\delta\Delta t/(1+z) = 10 \times 0.38/(1+0.84)$ light-days$\sim$ 2.1 light-days$= 5.4 \times 10^{15}$ cm, which corresponds to 1.2×10^3 times the Schwarzschild radius for a 1.5×10^7 $M_\odot$ BH ($R_s = 4.4 \times 10^{12}$ cm) and is larger than the rest-frame UV-optical emitting region.

3.3 Simultaneous Spectral Energy Distribution

The light curves sometimes show clear intranight variability by a factor of up to ~ 2, so the photometry used to construct SEDs should be almost simultaneous. All the colors and SEDs shown below are measured for data taken almost simultaneously, i.e., with time intervals shorter than 2 hours (0.083 days).

We made simultaneous SEDs at 10 epochs as shown in Figure 4, including instances during all the three observing epochs. We fit each SED with a single power-law ($f_\nu \propto \nu^{\alpha_\nu}$). The power-law indices α_ν are plotted as a function of observed or interpolated R_C-band brightness in Figure 5. In addition to fitting the photometric SEDs, the FOCAS and GMOS optical spectra were also fitted with a single power-law. We note that the fitting results for the FOCAS spectra ($\alpha_\nu = -1.40 \pm 0.01$) were presented in Tanaka et al. (2014). The obtained power-law index of the GMOS spectrum is $\alpha_\nu = -1.48 \pm 0.10$ but the spectrum is not corrected for the differential slit loss due to atmospheric differential refraction. The possible differential slit loss is about 20%, causing an overestimate of α_ν. We here do not estimate the exact factor and set the error of α_ν from the GMOS spectrum to be 0.3, roughly corresponding to the 20% difference. (i.e., $\alpha_\nu = -1.48 \pm 0.30$ instead of $\alpha_\nu = -1.48 \pm 0.10$).

These fitting results for the spectra are included in Figure 5.

Overall, the obtained power-law indices are consistent with being identical, although some of the indices are somewhat steep (small α_ν). This indicates that the origin of the optical-NIR emission (or spectrum) is the same regardless of brightness and observing epochs. The weighted average of the indices among our own monitoring data is $\alpha_\nu = -1.39 \pm 0.02$ as shown in gray shade in Figure 5.

In addition to our data, archival mid-infrared (MIR) data obtained with Wide-Field Infrared Survey Explorer (WISE) in the 3.4 μm (W1) and 4.6 μm-bands (W2) are available. These data were taken during the NEOWISE Reactivation mission (Mainzer et al. 2014). We made WISE light curves of J1100+4421 and nearby reference objects from the *Single Exposure (L1b) Source Table*. The WISE magnitudes in the Vega system obtained from the catalogs are converted to AB magnitudes using the equations in Jarrett et al. (2011), $W1_{\rm AB} = W1_{\rm Vega} + 2.699$ and $W2_{\rm AB} = W2_{\rm Vega} + 3.339$. By combining this with the WISE data shown in Tanaka et al. (2014), J1100+4421 shows clear variability around 56984 (Nov. 23, 2014) both in the W1 and W2 bands (Figure 6), while the reference objects are stable in flux within the error bars. The power-law indices derived from the two-band WISE data are $\alpha_{\nu,\rm MIR} \sim -1.4$ at all epochs. On days of MJD$= 56983 - 4$, the optical-MIR power-law index are also $\alpha_{\nu,\rm opt,MIR} \sim -1.4$.

3.4 Host Galaxy and Environment

Host galaxies of blazars are known to be massive elliptical galaxies (Sbarufatti et al. 2005; Falomo et al. 2014) while those of radio-loud NLS1 galaxies are star-forming galaxies (Zhou et al. 2007; Antón et al. 2008; León Tavares et al. 2014 Caccianiga et al. 2015). The central BH mass of J1100+4421 is measured using the Hβ and Mg$_{\rm II}$ emission lines and found to be as small as $1.0 - 1.5 \times 10^7$ M$_\odot$ (Tanaka et al. 2014). Considering this small BH mass, the host galaxy properties are expected to be similar to those of RLNLS1, rather than those of blazars. In addition, a large spatial extension of radio emission from this host galaxy is detected in FIRST data (Becker et al. 1995). We investigate here the host galaxy properties using the Subaru HSC images with sub-arcsec spatial resolution (see Figure 7).

The seeing sizes (FWHM) of the Subaru HSC images are 0.56 arcsec in g-band and 0.51 arcsec in z-band. The FWHM sizes of the object are 0.58 arcsec in g-band and 0.55 arcsec in z-band. These are almost unresolved and dominated by the nucleus. We note that the HSC magnitudes are $g = 21.71 \pm 0.12$ mag and $z = 20.57 \pm 0.11$ mag, respectively, both of are ~ 0.4 mag brighter than the SDSS magnitudes, which have photometric uncertainties of $\Delta g = 0.11$ and $\Delta z = 0.25$. We also note that these two HSC observations were done at different epochs.

Compared with the extended (~ 10 arcsec; Gabányi et al. 2017) radio emission detected in the FIRST data, the optical sizes measured above are much smaller. However, the optical sizes are measured using broad-band imaging data, and most of the light is continuum emission, including components from the AGN and the host galaxy. In the z-band bandpass, [O III] emission lines are included as well as the Hβ emission line, and we here set a brightness constraint on the extended [O III] emission. As seen in the HSC z-band image, no extended structure aligned to the radio structure is detected. Considering the width of the bandpass, we convert the upper limit of z-band surface brightness $z_{\rm lim} = 29.4$ [mag arcsec^{-2}] (3σ) to the upper limit of [O III] surface brightness $m([{\rm O\ III}])_{\rm lim} = 24.4$ [mag arcsec^{-2}] (3σ) by assuming that the [O III] spectral widths are the same (~ 10Å FWHM) as that of the central source spectrum. This limit corresponds to a flux density of 2.1×10^{-18} [erg s^{-1} cm^{-2} arcsec^{-2}] and is smaller than the [O III] flux detected for the central source by a factor of ~ 600. In addition to the imaging data, we examine the spatial extension of the [O III] emission lines along the slits detected in our spectroscopic data with FOCAS and GMOS. The sizes perpendicular to the slits are almost the same as or slightly extended than those of the continua, also indicating that the [O III] emitting region size is not as large as that in radio wavelength. We also note that there are no clear blue-shifted [O III] emission lines in any of our FOCAS and GMOS spectra.

4 Discussion

4.1 Contributions from Host Galaxy and Accretion Disk

We first evaluate the luminosity contribution of the host galaxy and the accretion disk. We note that the observed wavelength range corresponds to 0.2 μm to 1.2 μm in the rest-frame, UV to short NIR wavelengths.

The spectra do not show any significant absorption lines which could indicate host galaxy components. The faintest photometry among all of our data are the 5-band SDSS values. Although the measurement errors are not small ($\Delta m = 0.11 - 0.40$ mag), the measurements in the five different bands are almost simultaneous, the observation times ranging from MJD$= 52722.1509$ to MJD$= 52722.1542$ (48 minutes difference on March 23, 2004), and the fitted power-law index is $\alpha_\nu = -1.48 \pm 0.42$ (the leftmost point in the left panel of Figure 5); this is consistent with the power-law indices computed at other epochs. Although there is a possibility that the host galaxy color is similar to that of the varying AGN component, the contribution from the host galaxy, especially during the bright phases when we detected it with 1-2m class telescopes, is expected to be small. This is consistent with the fact

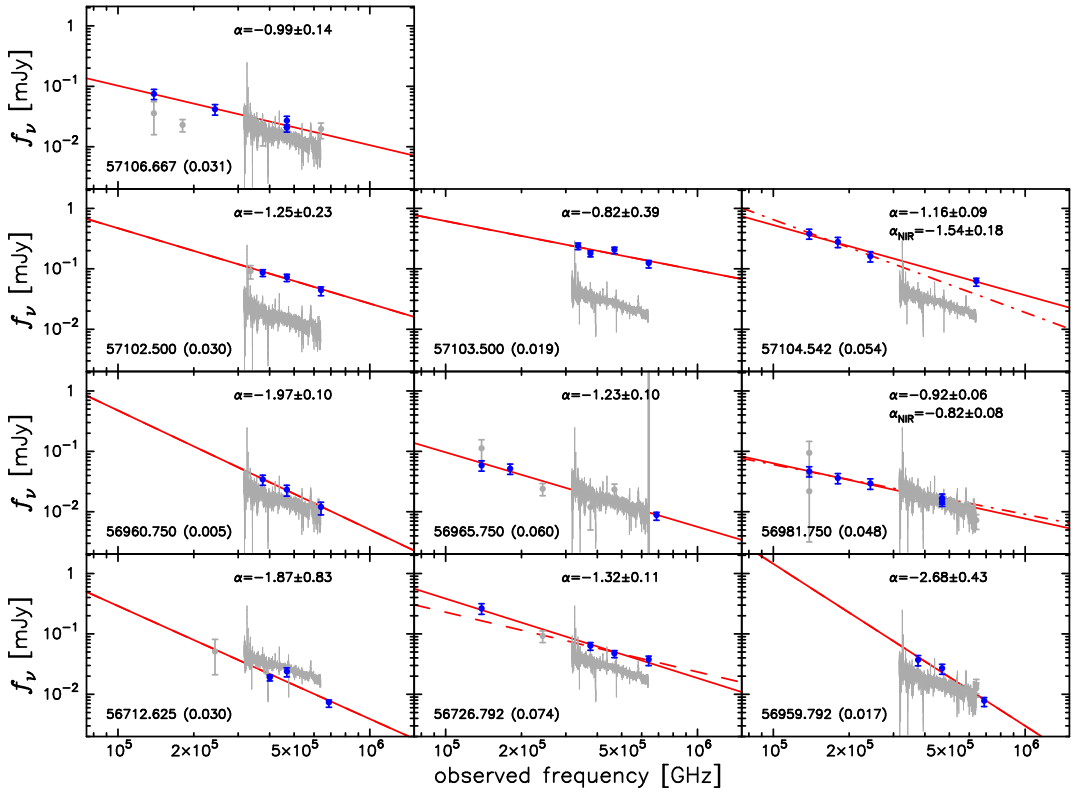

Fig. 4. The SEDs from NIR to optical during the simultaneous observations in blue filled circles. Observing times in MJD are shown in bottom-left and the time baseline among the observing points are shown in the parenthesis in a unit of day. The fitted lines are shown in red. Note that gray filled circles are data points with low signal-to-noise ratios (S/N<3) and not used for the fitting. Solid, dashed, and dot-dashed lines indicate that the SEDs in NIR and optical, optical, and NIR wavelengths are fitted. The FOCAS spectra in the two phases ($\alpha_{\nu,\rm opt}=-1.40$, the brightest and faintest) are also shown in gray alternately for a reference purpose. The Galactic extinction are corrected for the data points and power-law indices calculated here.

that host galaxies (bulge components) of low-z NLS1s are as faint as $M_{B,\rm bulge}=-18.5$ mag (Botte et al. 2004), corresponding to $m_i\sim25.2$ mag at this redshift, much fainter than the detection limits of most of our data.

The second item to be examined is the luminosity of the accretion disk. The BH mass is estimated to be $1.0-1.5\times10^7$ $M_\odot$, based on the line luminosity and widths of the Mg II and Hβ emission lines (Tanaka et al. 2014). The bolometric luminosity can be explained by sub-Eddington accretion ($\sim30\%$). For a BH with this small mass and normal (or somewhat high) Eddington ratio, the peak wavelength of the accretion disk semi-blackbody emission is UV to soft X-ray if we assume that the object has a standard accretion disk (Shakura & Sunyaev 1973). This means that the luminosity of the UV-optical wavelength region is expected to be $f_\nu\propto\nu^{1/3}$ ($\alpha_\nu=1/3$) which is inconsistent with, much harder than, the obtained power-law index $\alpha_\nu\sim-1.4$. This indicates the accretion disk component does not significantly contribute to the observed flux in the observed wavelength range.

4.2 Synchrotron Radiation in optical-NIR Wavelength Regions

Considering the small luminosity contribution from the host galaxy and accretion disk, a plausible explanation for the varying luminosity with constant power-law indices would be synchrotron emission by high-energy electrons inside a relativistic jet.

Following the conventional synchrotron theory (see Rybicki & Lightman 1979 for details), we can derive the power-law index of electron distribution ($dN_e/dE\propto E^{-p}$) from the observed optical-IR spectrum as $p=-2\alpha+1=3.8$. This is much softer than the prediction of standard diffusive shock acceleration theory, which predicts the power-law index of $p=2.0$ (e.g, Blandford & Ostriker 1978). We note that such a soft electron distribution is easily achieved by e.g., radiative cooling, inefficient acceleration and so on, and hence the electron power-law index of ~3.8 estimated here is not unusual. Indeed, it is well known that similar soft electron distribution is derived in many blazars by applying synchrotron plus inverse-Compton modeling of the broad-band spectral energy distribution from radio to γ-ray (see e.g, Ghisellini et al. 2010).

The emission mechanism can be investigated with higher-

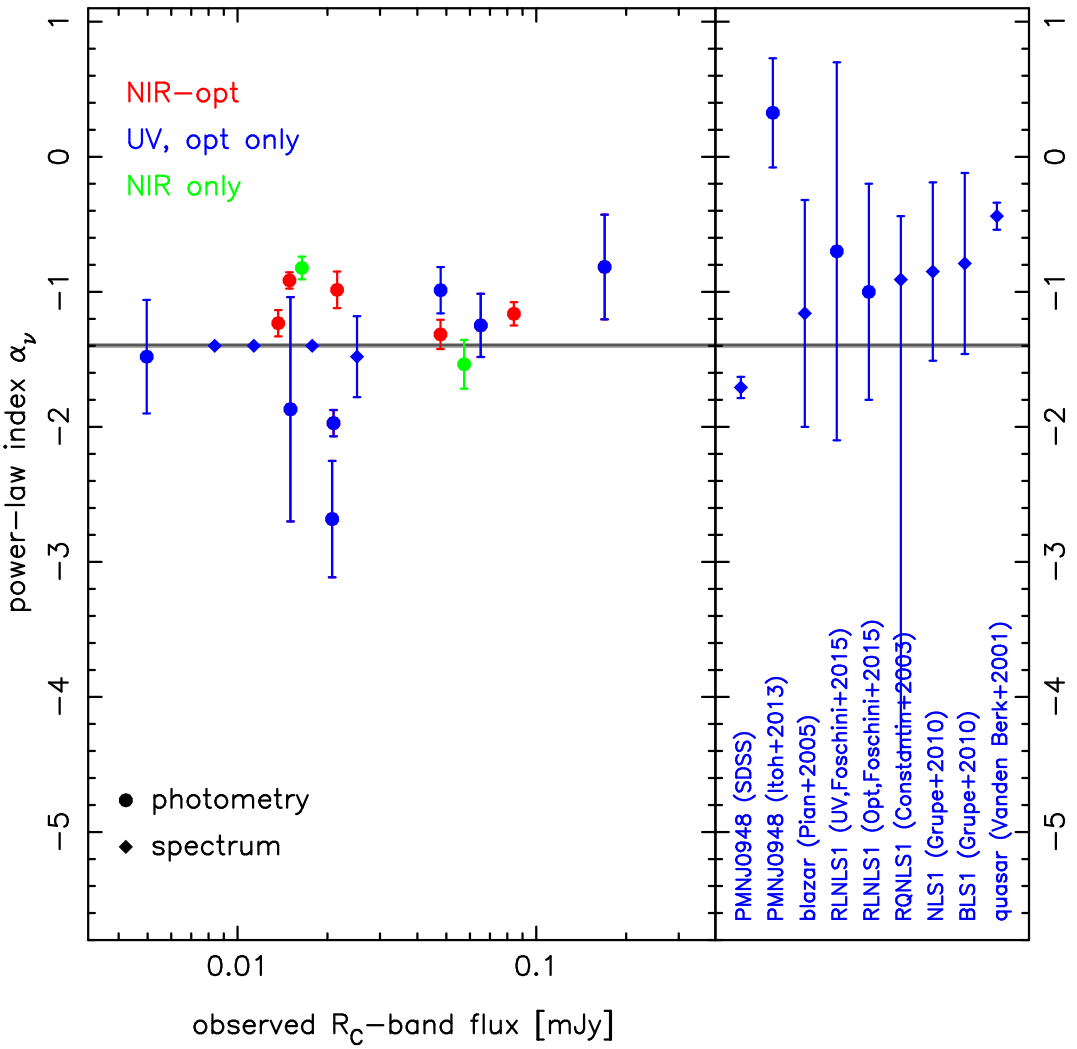

Fig. 5. *(Left)*: Power-law index versus R_C-band flux for SDSS J1100+4421. Filled circles are values obtained with the simultaneous imaging data. Different colors (red, blue, and green) indicate different wavelength ranges (optical and NIR, optical and NIR in the observed frame) fitted to calculated the power-law indices. Filled boxes indicate the power-law indices obtained from the FOCAS and GMOS spectra. The leftmost filled circle is the power-law index from the SDSS photometry. The averaged α_ν is shown in gray shaded region. The Galactic extinction are corrected when we calculate the power-law indices. *(Right)*: Power-law indices of various kinds of AGN from the literature. Indices of the optical SDSS spectrum of PMN J0948+0022, optical imaging of PMN J0948+0022 (Itoh et al. 2013), UV spectra of blazars (Pian et al. 2005), UV imaging of radio-loud NLS1s (Foschini et al. 2015), optical spectra of radio-loud NLS1s (Foschini et al. 2015), UV spectra of radio-quiet NLS1s (Constantin & Shields 2003), UV imaging of narrow-line and broad line Seyferts (Grupe et al. 2010), and optical SDSS spectra of quasars (Vanden Berk et al. 2001) are shown. The bars indicate the root-mean-square of α_ν for Grupe et al. (2010), the systematic uncertainty of α_ν for quasars (Vanden Berk et al. 2001), and the ranges of the α_ν values for the rest of the papers.

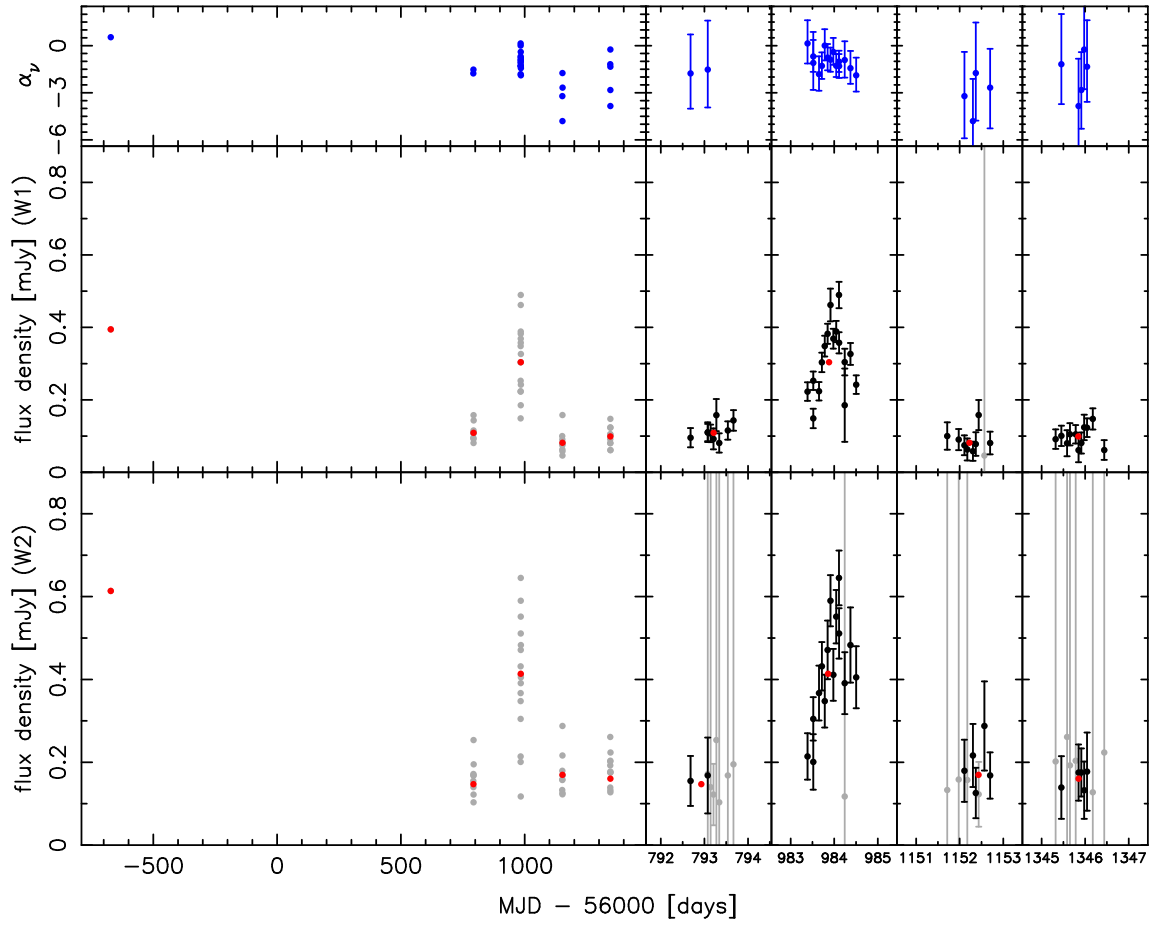

Fig. 6. *(Top)*: Power-law indices calculated with the WISE 3.4 μm and 4.6 μm-band data as a function of time. *(Middle), (Bottom)*: WISE light curves of J1100+4421 in the 3.4 μm (W1) and 4.6 μm (W2) -bands are shown in gray. The left panels are for the whole range of the WISE data while the other panels are magnified views of the four observing epochs of the NEOWISE Reactivation mission. In the four right panels, data points with < 0.5 mag errors are shown in black. Weighted averages of flux during each epoch is shown in red. The error bars are shown only in the magnified panels.

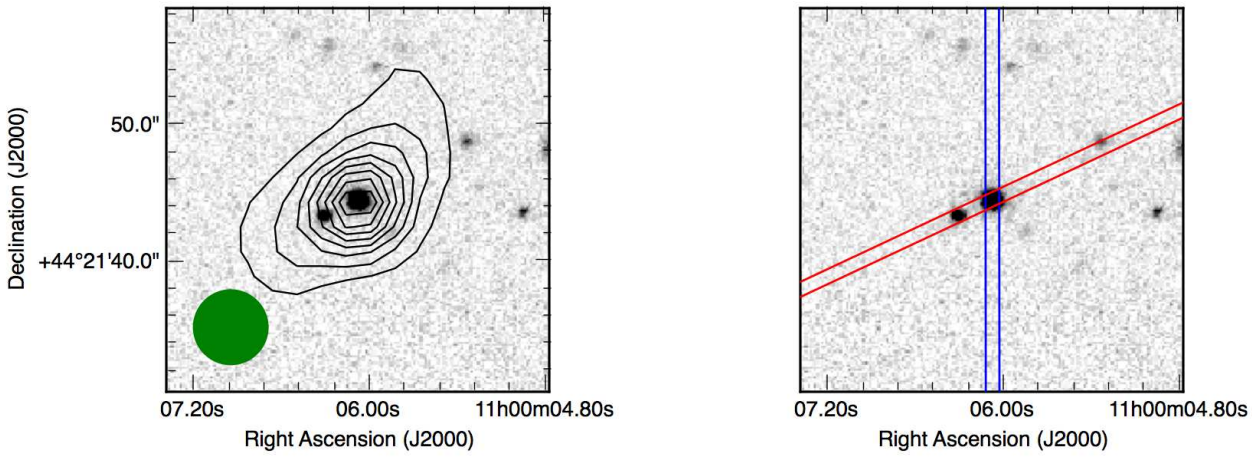

Fig. 7. *(Left)*: Subaru/HSC z-band image in gray scale overlaid with the FIRST radio data in contour. The central object in this figure is J1100+4421. Beam size of the FIRST image (5.4 arcsec) is shown at the left-bottom part of the figure in green. *(Right)*: The slits of the FOCAS and GMOS observations are shown in blue and red, respectively.

energy observational data where the synchrotron self-Compton (SSC) radiation dominates. We checked Fermi Large Area Telescope (LAT) source catalog (3FGL; Fermi LAT 4-Year Point Source Catalog; Acero et al. 2015) and found that no object is detected at the position of J1100+4421; and no source appears in the 2FGL catalog investigated in Tanaka et al. (2014). The Fermi/LAT upper limit in νF_ν units is a few times 10^{-12} erg s^{-1} cm^{-2} (Acero et al. 2015). This upper limit is roughly comparable to the expected SSC emission and can be explained by the synchrotron/SSC model (Chiang & Böttcher 2002) if we assume $p = 3.8$.

The observed optical-NIR SEDs are well described by synchrotron emission, which indicates that the peak frequency of the synchrotron emission is lower than the observed wavelength range, $\nu_{\rm peak} < 10^{15}$ Hz, and so the object belongs to a low-frequency-peaked blazar population. The observed optical-NIR colors of J1100+4421 at $z = 0.840$, obtained almost simultaneously, are $g - J \sim 1.1$, $R - J \sim 0.8$, and $I - J \sim 0.6$ in the AB system, roughly corresponding to $g - J \sim 2.1$, $R - J \sim 1.5$, and $I - J \sim 1.1$ in the Vega system. These colors are at the blue end of the distribution for blazars at $z \sim 0.02 - 1.8$ shown in Ikejiri et al. (2011) and consistent with both the colors of higher- or lower-frequency-peaked populations. The large variability amplitude ($\Delta g \sim 3.5$ mag, a factor of ~ 30, between the SDSS and our March 2015 photometry) also might indicate that J1100+4421 is similar to low $\nu_{\rm peak}$ blazars because there are no high $\nu_{\rm peak}$ blazars showing such a large amplitude of variability (Ikejiri et al. 2011). The small color variability within our observations, i.e. almost constant power-law indices, is consistent with the object belonging to a low $\nu_{\rm peak}$ blazar population.

A comparison with the spectral indices of other AGN is shown in the right panel of Figure 5. The power-law index α_ν of J1100+4421 in the rest-frame UV to short NIR wavelengths is consistent with those in the observed UV wavelengths for blazars at $z = 0.15 - 1.41$ ($\alpha_{\nu,\rm UV} = -2.00$–$-0.32$; Pian et al. 2005), RLNLS1 at $z = 0.06 - 0.80$ ($\alpha_{\nu,\rm UV} = -0.7 \pm 1.4$, median -0.7; Foschini et al. 2015), RLNLS1 at $z = 0.06 - 0.80$ ($\alpha_{\nu,\rm opt} = --1.0 \pm 0.8$, median -0.8; Foschini et al. 2015), RQNLS1 at $z = 0.01 - 0.26$ ($\alpha_{\nu,\rm UV} = -4.41$–$-0.44$, median -0.91; Constantin & Shields 2003), broad-line Seyferts at $< z >= 0.086$ ($\alpha_{\nu,\rm UV} = -0.79 \pm 0.67$, median -0.61; Grupe et al. 2010), and narrow-line Seyferts at $< z >= 0.087$ ($\alpha_{\nu,\rm UV} = -0.85 \pm 0.66$, median -0.65; Grupe et al. 2010) We note that most of these values are the range of the α_ν values, not the root-mean-square, except for the values in Grupe et al. (2010). On the other hand, the power-law index of J1100+4421 is clearly different from those of SDSS quasars ($\alpha_\nu = -0.44$, ~ 0.1 uncertainty) shown in Vanden Berk et al. (2001) and most ($> 90\%$) of the SDSS quasars have harder UV-optical spectra than J1100+4421 (Shen et al. 2011). This difference also supports our hypothesis that the emission of J1100+4421 in optical-NIR wavelength regions arises from synchrotron radiation in the relativistic jet, not an accretion disk.

The famous Fermi LAT-detected NLS1, PMN J0948+0022 (Abdo et al. 2009a), a low $\nu_{\rm peak}$ radio/γ-loud NLS1 at $z = 0.585$, shares observational properties similar to J1100+4421 including kpc-scale radio emission (Doi et al. 2012), but lacks the high [O III]/Hβ flux ratio of J1100+4421. If J1100+4421 follows the general distributions observed for low $\nu_{\rm peak}$ blazars in Ikejiri et al. (2011), a high degree of polarization might be expected for J1100+4421 as was indeed detected from PMN J0948+0022 (Itoh et al. 2013).

PMN J0948+0022 shows a different behavior in its power-law indices than J1100+4421. The extinction-corrected ($A_V = 0.263$ mag; Schlegel et al. 1998; assuming the extinction law given by Cardelli et al. 1989) SDSS spectrum of PMN J0948+0022 gives a power-law index $\alpha_\nu = -1.77 \pm 0.07$. On the other hand, Itoh et al. (2013) measured an optical power-law index of $0 < \alpha_\nu < 1$ during a brighter phase of PMN J0948+0022 after the detection of a γ-ray flare with Fermi LAT. They indicated that the index varies at different brightness phases, which is a well known behavior known as the "bluer-when-brighter" trend for blazars (e.g., Ikejiri et al. 2011) and quasars (e.g., Kokubo et al. 2014); we note that J1100+4421 does not show such a change in its power-law indices.

4.3 Host Galaxy and Environment

As pointed out in previous papers, there is a hypothesis that radio-loud NLS1s, which are an AGN population mostly similar to J1100+4421, are products of interaction (Zhou et al. 2007; Antón et al. 2008). Therefore, we consider here whether or not this hypothesis is valid for J1100+4421. For more massive systems like quasars, the existence of extended narrow emission line regions sometimes indicates recent minor merger events and AGN triggering (Fu & Stockton 2009; Matsuoka 2012). An observational study on extended narrow-line regions in nearby Seyfert galaxies (Keel et al. 2012) also shows that a significant fraction of the sample galaxies are interacting or merging systems. However, as shown in Section 3.4, we tentatively conclude that an extended [O III] emitting region is *not* present in our optical broad-band imaging data.

This indicates the small (< 1 arcsec FWHM corresponding to several kpc) size of the [O III] emitting regions. This small size of the [O III] narrow-line region itself is partly consistent with the notion that large, extended narrow-line regions are usually associated with AGN which have low Eddington ratios and/or high BH masses (Matsuoka 2012).

The power-law index of this object in the radio frequency is hard to measure because of non-simultaneous observations as shown in Table 1 of Tanaka et al. (2014). The indices naively measured (i.e., ignoring the time differences between the obser-

vations) indicate both possibilities that J1100+4421 belongs to flat- or steep-spectrum population. If J1100+4421 is a steep-spectrum radio-loud AGN which is indicated by the largely extended radio lobe, the radio-loud nature, which is one of the unique points of J1100+4421, may be inconsistent with the fact that a high fraction (about 60%) of steep-spectrum radio-loud quasars may host extended narrow-line regions, although not all of them do (Matsuoka 2012).

We identified a galaxy at (RA, Dec) = (11:00:06.30, +44:21:43.4), to the east of J1100+4421 by 2.7 arcsec (21 kpc at this redshift, $z = 0.840$) in our deep HSC imaging data. The magnitudes of this galaxy are $g = 25.32 \pm 0.36$ mag and $z = 22.15 \pm 0.09$ mag in Novermber 2014, a factor of 18.4 and 3.0 fainter than the faintest phases of J1100+4421, respectively. We took a GMOS optical spectrum of this galaxy with a 1.0 arcsec-width slit along J1100+4421 as described in Section 2.2.1. The spectrum does not show any significant continuum because of the faintness of the galaxy and the short exposure, and does not show any emission lines at the same redshift as that of J1100+4421. Hence it is unclear whether or not this galaxy interacts with J1100+4421. As pointed by Doi et al. (2012), RLNLS1s with extended radio structure, with which J1100+4421 shares similar properties, are thought to be at the final stage of evolution of NLS1s, possibly as they evolve to broad-line, more massive, AGN. With this hypothesis in mind, the possible non-detection of extended narrow-line regions might be consistent with preferred detections in massive systems.

5 Summary

We carried out monitoring campaign observations at optical and NIR wavelengths for the radio-loud AGN J1100+4421 with a BH mass of $1.0 - 1.5 \times 10^7$ $M_\odot$. The light curves and simultaneous SEDs are shown and rapid variability behaviors are detected in each of the three observing campaigns. The object shows large variability during our observations, changing by a factor of ~ 30 while its power-law indices remain unchanged ($\alpha_\nu \sim -1.4$ where $f_\nu \propto \nu^{\alpha_\nu}$). All of the observational results are consistent with the hypothesis that the optical-NIR emission originates from synchrotron radiation in a relativistic jet. The small SED changes indicate that J1100+4421 belongs to a low $\nu_{\rm peak}$ blazar population. The marginal spatial resolution in sub-arcsec optical imaging data taken with Subaru HSC, showing no large, extended [O III] narrow-line region, is smaller than the extended radio emission detected in the FIRST survey data. A newly obtained optical spectrum of a possible companion galaxy does not support the idea that the galaxy is at the same redshift of J1100+4421, or the merging hypothesis for triggering the AGN-related activity of J1100+4421. To understand the nature of J1100+4421, which does not share all its properties with any other set of objects like NLS1s, further observations including multi-wavelength, high-resolution radio VLBI (Gabányi et al. 2017), deep narrow-line region imaging or integral-field spectroscopy, more densely-sampled monitoring, and polarization are required.

Acknowledgments

This work was supported by the Optical and Near-infrared Astronomy Inter-University Cooperation Program and the Grants-in-Aid of the Ministry of Education, Science, Culture, and Sport 23740143, 25800103, 16H02158 15H02075, 15H00788, 24740117, 25103515, 23740157, 15J10324, 19047003, 25707007. This work was partially carried out by the joint research program of the Institute for Cosmic Ray Research (ICRR), University of Tokyo, based in part on data collected at Subaru Telescope, which is operated by the National Astronomical Observatory of Japan and data obtained at the Gemini Observatory via the time exchange program between Gemini and the Subaru Telescope, and also based on data obtained by SDSS-III. The Gemini Observatory is operated by the Association of Universities for Research in Astronomy, Inc., under a cooperative agreement with the NSF on behalf of the Gemini partnership: the National Science Foundation (United States), the National Research Council (Canada), CONICYT (Chile), Ministerio de Ciencia, Tecnología e Innovación Productiva (Argentina), and Ministério da Ciência, Tecnologia e Inovação (Brazil). SDSS-III is managed by the Astrophysical Research Consortium for the Participating Institutions of the SDSS-III Collaboration including the University of Arizona, the Brazilian Participation Group, Brookhaven National Laboratory, Carnegie Mellon University, University of Florida, the French Participation Group, the German Participation Group, Harvard University, the Instituto de Astrofisica de Canarias, the Michigan State/Notre Dame/JINA Participation Group, Johns Hopkins University, Lawrence Berkeley National Laboratory, Max Planck Institute for Astrophysics, Max Planck Institute for Extraterrestrial Physics, New Mexico State University, New York University, Ohio State University, Pennsylvania State University, University of Portsmouth, Princeton University, the Spanish Participation Group, University of Tokyo, University of Utah, Vanderbilt University, University of Virginia, University of Washington, and Yale University. This publication makes use of data products from the Two Micron All Sky Survey, which is a joint project of the University of Massachusetts and the Infrared Processing and Analysis Center/California Institute of Technology, funded by the National Aeronautics and Space Administration and the National Science Foundation. This paper makes use of software developed for the Large Synoptic Survey Telescope. We thank the LSST Project for making their code available as free software at http://dm.lsstcorp.org. Funding for SDSS-III has been provided by the Alfred P. Sloan Foundation, the Participating Institutions, the National Science Foundation, and the U.S. Department of Energy Office of Science. The SDSS-III web site is http://www.sdss3.org/.

We also appreciate a kind help by Prof. Michael W. Richmond for improving the English grammar of the manuscript and a private communication with Dr. Luigi Foschini.

References

Abdo, A. A., Ackermann, M., Ajello, M., et al. 2009a, ApJ, 699, 976

—. 2009b, ApJL, 707, L142

Acero, F., Ackermann, M., Ajello, M., et al. 2015, ApJS, 218, 23
Akitaya, H., Moritani, Y., Ui, T., et al. 2014, in Proc. SPIE, Vol. 9147, Ground-based and Airborne Instrumentation for Astronomy V, 91474O
Alam, S., Albareti, F. D., Allende Prieto, C., et al. 2015, ApJS, 219, 12
Antón, S., Browne, I. W. A., & Marchã, M. J. 2008, A&A, 490, 583
Axelrod, T., Kantor, J., Lupton, R. H., & Pierfederici, F. 2010, in Proc. SPIE, Vol. 7740, Software and Cyberinfrastructure for Astronomy, 774015
Becker, R. H., White, R. L., & Helfand, D. J. 1995, ApJ, 450, 559
Berton, M., Foschini, L., Ciroi, S., et al. 2016, A&A, 591, A88
Blandford, R. D., & Ostriker, J. P. 1978, ApJL, 221, L29
Botte, V., Ciroi, S., Rafanelli, P., & Di Mille, F. 2004, AJ, 127, 3168
Caccianiga, A., Antón, S., Ballo, L., et al. 2015, MNRAS, 451, 1795
Cardelli, J. A., Clayton, G. C., & Mathis, J. S. 1989, ApJ, 345, 245
Chiang, J., & Böttcher, M. 2002, ApJ, 564, 92
Constantin, A., & Shields, J. C. 2003, PASP, 115, 592
Doi, A., Nagira, H., Kawakatu, N., et al. 2012, ApJ, 760, 41
Falomo, R., Pian, E., & Treves, A. 2014, A&AR, 22, 73
Fan, J., Yang, J. H., Zhang, J.-Y., et al. 2013, PASJ, 65, 25
Foschini, L., Ghisellini, G., Tavecchio, F., Bonnoli, G., & Stamerra, A. 2011, A&A, 530, A77
Foschini, L., Berton, M., Caccianiga, A., et al. 2015, A&A, 575, A13
Fu, H., & Stockton, A. 2009, ApJ, 690, 953
Gabányi, K. É., Frey, S., Paragi, Z., et al. 2017, submitted to MNRAS
Ghisellini, G., Tavecchio, F., Foschini, L., et al. 2010, MNRAS, 402, 497
Grupe, D., Komossa, S., Leighly, K. M., & Page, K. L. 2010, ApJS, 187, 64
Hashiba, Y., Doi, M., Sako, S., et al. 2014, in Proc. SPIE, Vol. 9147, Ground-based and Airborne Instrumentation for Astronomy V, 91472J
Hook, I. M., Jørgensen, I., Allington-Smith, J. R., et al. 2004, PASP, 116, 425
Ikejiri, Y., Uemura, M., Sasada, M., et al. 2011, PASJ, 63, 639
Itoh, R., Tanaka, Y. T., Fukazawa, Y., et al. 2013, ApJL, 775, L26
Ivezic, Z., Tyson, J. A., Abel, B., et al. 2008, ArXiv e-prints, arXiv:0805.2366
Jarrett, T. H., Cohen, M., Masci, F., et al. 2011, ApJ, 735, 112
Jester, S., Schneider, D. P., Richards, G. T., et al. 2005, AJ, 130, 873
Kashikawa, N., Aoki, K., Asai, R., et al. 2002, PASJ, 54, 819
Keel, W. C., Chojnowski, S. D., Bennert, V. N., et al. 2012, MNRAS, 420, 878
Kokubo, M., Morokuma, T., Minezaki, T., et al. 2014, ApJ, 783, 46
Kotani, T., Kawai, N., Yanagisawa, K., et al. 2005, Nuovo Cimento C Geophysics Space Physics C, 28, 755
León Tavares, J., Kotilainen, J., Chavushyan, V., et al. 2014, ApJ, 795, 58
Mainzer, A., Bauer, J., Cutri, R. M., et al. 2014, ApJ, 792, 30
Matsuoka, Y. 2012, ApJ, 750, 54
Miyazaki, S., Komiyama, Y., Nakaya, H., et al. 2012, in Proc. SPIE, Vol. 8446, Ground-based and Airborne Instrumentation for Astronomy IV, 84460Z
Morokuma, T., Tominaga, N., Tanaka, M., et al. 2014, PASJ, 66, 114
Pian, E., Falomo, R., & Treves, A. 2005, MNRAS, 361, 919
Rybicki, G. B., & Lightman, A. P. 1979, Radiative processes in astrophysics
Saito, Y., Morokuma, T., Akitaya, H., et al. 2017, in prep.
Sakimoto, K., Akitaya, H., Yamashita, T., et al. 2012, in Proc. SPIE, Vol. 8446, Ground-based and Airborne Instrumentation for Astronomy IV, 844673
Sako, S., Aoki, T., Doi, M., et al. 2012, in Proc. SPIE, Vol. 8446, Ground-based and Airborne Instrumentation for Astronomy IV, 84466L
Sbarufatti, B., Treves, A., & Falomo, R. 2005, ApJ, 635, 173
Schlafly, E. F., & Finkbeiner, D. P. 2011, ApJ, 737, 103
Schlegel, D. J., Finkbeiner, D. P., & Davis, M. 1998, ApJ, 500, 525
Sekiguchi, K., Akitaya, H., Kuroda, D., et al. 2017, in prep.
Shakura, N. I., & Sunyaev, R. A. 1973, A&A, 24, 337
Shen, Y., Richards, G. T., Strauss, M. A., et al. 2011, ApJS, 194, 45
Shimokawabe, T., Kawai, N., Kotani, T., et al. 2008, in American Institute of Physics Conference Series, Vol. 1000, American Institute of Physics Conference Series, ed. M. Galassi, D. Palmer, & E. Fenimore, 543–546
Skrutskie, M. F., Cutri, R. M., Stiening, R., et al. 2006, AJ, 131, 1163
Tanaka, M., Morokuma, T., Itoh, R., et al. 2014, ApJL, 793, L26
Tokunaga, A. T., & Vacca, W. D. 2005, PASP, 117, 421
Urry, C. M., Treves, A., Maraschi, L., et al. 1997, ApJ, 486, 799
Vanden Berk, D. E., Richards, G. T., Bauer, A., et al. 2001, AJ, 122, 549
Watanabe, M., Takahashi, Y., Sato, M., et al. 2012, in Proc. SPIE, Vol. 8446, Ground-based and Airborne Instrumentation for Astronomy IV, 84462O
Yanagisawa, K., Kuroda, D., Yoshida, M., et al. 2010, in American Institute of Physics Conference Series, Vol. 1279, American Institute of Physics Conference Series, ed. N. Kawai & S. Nagataki, 466–468
Yanagisawa, K., Okita, K., Shimizu, Y., et al. 2008, in Proc. SPIE, Vol. 7014, Ground-based and Airborne Instrumentation for Astronomy II, 701437
Yatsu, Y., Kawai, N., Shimokawabe, T., et al. 2007, Physica E Low-Dimensional Systems and Nanostructures, 40, 434
Yoshida, M. 2005, Journal of Korean Astronomical Society, 38, 117
Zhang, B. K., Dai, B. Z., Wang, L. P., et al. 2012, MNRAS, 421, 3111
Zhou, H., Wang, T., Yuan, W., et al. 2007, ApJL, 658, L13

Table 2. Summary of Optical and Near-Infrared Photometric Measurements of J1100+4421. Galactic extinctions are not corrected.

telescope	instrument	filter	MJD	date (UT)	magnitude
Kiso	KWFC	u	56958.80	2014-10-28	> 20.27
Kiso	KWFC	u	56964.82	2014-11-03	> 20.41
Kiso	KWFC	u	56968.84	2014-11-07	> 18.86
Kiso	KWFC	u	56976.74	2014-11-15	> 19.56
Kiso	KWFC	u	56977.82	2014-11-16	> 20.36
Subaru	FOCAS	B	56712.27	2014-02-24	21.17 ± 0.10
Subaru	FOCAS	B	56712.55	2014-02-24	21.72 ± 0.10
Subaru	FOCAS	B	56712.63	2014-02-24	21.78 ± 0.10
Pirka	MSI	B	56954.82	2014-10-24	> 20.03
Pirka	MSI	B	56955.82	2014-10-25	> 16.95
Pirka	MSI	B	56959.80	2014-10-29	21.71 ± 0.14
Pirka	MSI	B	56965.78	2014-11-04	21.58 ± 0.12
Pirka	MSI	B	56983.84	2014-11-22	21.16 ± 0.14
Pirka	MSI	B	56984.83	2014-11-23	21.72 ± 0.16
Pirka	MSI	B	56986.84	2014-11-25	22.13 ± 0.21
Pirka	MSI	B	56987.83	2014-11-26	22.14 ± 0.15
Pirka	MSI	B	56988.79	2014-11-27	21.73 ± 0.16
Kottamia	Kottamia	B	57063.03	2015-02-10	> 19.93
Pirka	MSI	B	57174.58	2015-06-01	> 19.25
Pirka	MSI	B	57175.61	2015-06-02	> 16.22
Kiso	KWFC	g	56325.66	2013-02-02	> 21.33
Kiso	KWFC	g	56327.70	2013-02-04	> 21.06
Kiso	KWFC	g	56347.59	2013-02-24	> 18.67
Kiso	KWFC	g	56709.50	2014-02-21	> 20.90
Kiso	KWFC	g	56710.51	2014-02-22	> 21.30
Kiso	KWFC	g	56711.46	2014-02-23	19.73 ± 0.16
Kiso	KWFC	g	56711.51	2014-02-23	20.18 ± 0.13
Kiso	KWFC	g	56711.51	2014-02-23	20.22 ± 0.20
Kiso	KWFC	g	56711.55	2014-02-23	19.96 ± 0.15
Kiso	KWFC	g	56711.60	2014-02-23	19.82 ± 0.14
Kiso	KWFC	g	56712.72	2014-02-24	21.08 ± 0.14
Kiso	KWFC	g	56712.72	2014-02-24	21.19 ± 0.14
Kiso	KWFC	g	56713.63	2014-02-25	21.50 ± 0.14
Kiso	KWFC	g	56713.63	2014-02-25	21.48 ± 0.14
Kiso	KWFC	g	56714.46	2014-02-26	> 19.05
Kiso	KWFC	g	56718.70	2014-03-02	> 20.34
Kiso	KWFC	g	56726.82	2014-03-10	20.01 ± 0.15
Kiso	KWFC	g	56727.57	2014-03-11	> 20.62
Kiso	KWFC	g	56728.49	2014-03-12	> 18.48
Kiso	KWFC	g	56731.66	2014-03-15	> 20.23
Kiso	KWFC	g	56732.77	2014-03-16	> 19.84
Kiso	KWFC	g	56733.52	2014-03-17	> 20.04
Kiso	KWFC	g	56738.74	2014-03-22	> 20.68
Kiso	KWFC	g	56739.74	2014-03-23	> 20.86
Kiso	KWFC	g	56744.51	2014-03-28	> 20.85
Kiso	KWFC	g	56745.42	2014-03-29	> 16.95
Kiso	KWFC	g	56747.72	2014-03-31	> 21.07
Kiso	KWFC	g	56748.73	2014-04-01	> 20.00
Kiso	KWFC	g	56749.74	2014-04-02	> 21.11

Table 2. (Continued)

telescope	instrument	filter	MJD	date (UT)	magnitude
Kiso	KWFC	g	56765.58	2014-04-18	> 19.63
Kiso	KWFC	g	56766.49	2014-04-19	> 20.90
Kiso	KWFC	g	56770.60	2014-04-23	21.21 ± 0.20
Kiso	KWFC	g	56771.57	2014-04-24	> 21.72
Kiso	KWFC	g	56772.53	2014-04-25	> 21.32
Kiso	KWFC	g	56773.54	2014-04-26	> 20.73
Kiso	KWFC	g	56774.53	2014-04-27	> 21.72
Kiso	KWFC	g	56809.54	2014-06-01	> 21.39
Kiso	KWFC	g	56850.48	2014-07-12	> 18.33
Kiso	KWFC	g	56853.49	2014-07-15	> 21.06
Kiso	KWFC	g	56859.49	2014-07-21	> 20.43
Kiso	KWFC	g	56876.47	2014-08-07	> 18.75
Kiso	KWFC	g	56946.84	2014-10-16	> 18.70
Akeno	MITSuME	g	56954.73	2014-10-24	> 19.87
Akeno	MITSuME	g	56955.73	2014-10-25	> 20.75
Akeno	MITSuME	g	56957.73	2014-10-27	> 19.09
OAO	MITSuME	g	56957.80	2014-10-27	> 20.59
Kiso	KWFC	g	56957.80	2014-10-27	> 20.57
Akeno	MITSuME	g	56958.72	2014-10-28	> 20.72
Kiso	KWFC	g	56958.78	2014-10-28	> 21.17
OAO	MITSuME	g	56958.80	2014-10-28	> 20.06
Kiso	KWFC	g	56959.78	2014-10-29	> 21.55
Murikabushi	MITSuME	g	56959.80	2014-10-29	> 21.38
OAO	MITSuME	g	56959.84	2014-10-29	> 19.20
Murikabushi	MITSuME	g	56960.78	2014-10-30	21.24 ± 0.22
Kiso	KWFC	g	56960.80	2014-10-30	> 21.07
Murikabushi	MITSuME	g	56961.78	2014-10-31	> 21.02
Akeno	MITSuME	g	56962.73	2014-11-01	> 20.93
Akeno	MITSuME	g	56963.71	2014-11-02	> 20.18
OAO	MITSuME	g	56963.83	2014-11-02	> 19.36
Akeno	MITSuME	g	56964.73	2014-11-03	> 20.70
Kiso	KWFC	g	56964.79	2014-11-03	> 21.41
OAO	MITSuME	g	56964.83	2014-11-03	> 20.31
Kiso	KWFC	g	56965.76	2014-11-04	> 20.09
Akeno	MITSuME	g	56965.78	2014-11-04	> 20.00
OAO	MITSuME	g	56965.83	2014-11-04	> 20.14
Akeno	MITSuME	g	56967.73	2014-11-06	> 19.89
Kiso	KWFC	g	56967.79	2014-11-06	> 19.90
OAO	MITSuME	g	56967.85	2014-11-06	> 18.55
Akeno	MITSuME	g	56968.78	2014-11-07	> 20.07
Kiso	KWFC	g	56968.82	2014-11-07	> 20.33
Kiso	KWFC	g	56970.81	2014-11-09	> 20.67
OAO	MITSuME	g	56971.83	2014-11-10	> 19.64
Akeno	MITSuME	g	56973.70	2014-11-12	> 20.53
Akeno	MITSuME	g	56974.69	2014-11-13	> 20.61
Akeno	MITSuME	g	56975.68	2014-11-14	> 20.82
Akeno	MITSuME	g	56976.68	2014-11-15	> 20.92
Kiso	KWFC	g	56976.72	2014-11-15	> 20.60
Akeno	MITSuME	g	56977.67	2014-11-16	> 20.64

Table 2. (Continued)

telescope	instrument	filter	MJD	date (UT)	magnitude
Akeno	MITSuME	g	56978.72	2014-11-17	> 20.56
Akeno	MITSuME	g	56979.66	2014-11-18	> 21.07
Akeno	MITSuME	g	56980.69	2014-11-19	> 20.00
Murikabushi	MITSuME	g	56980.72	2014-11-19	> 20.55
Akeno	MITSuME	g	56981.66	2014-11-20	> 21.00
Kiso	KWFC	g	56981.69	2014-11-20	> 21.82
Murikabushi	MITSuME	g	56981.73	2014-11-20	> 21.42
Kiso	KWFC	g	56982.76	2014-11-21	> 21.15
Kiso	KWFC	g	56983.74	2014-11-22	20.56 ± 0.20
Nayuta	LISS	g	56984.50	2014-11-23	> 20.19
Kiso	KWFC	g	56984.72	2014-11-23	> 21.47
Kiso	KWFC	g	56987.81	2014-11-26	> 21.44
Subaru	HSC	g	56988.50	2014-11-27	21.72 ± 0.12
Kiso	KWFC	g	56988.67	2014-11-27	> 21.50
Murikabushi	MITSuME	g	56989.71	2014-11-28	> 20.34
Kiso	KWFC	g	57009.83	2014-12-18	19.51 ± 0.12
Kiso	KWFC	g	57014.60	2014-12-23	> 18.98
Kiso	KWFC	g	57040.57	2015-01-18	> 19.53
Kiso	KWFC	g	57042.60	2015-01-20	> 21.47
Kiso	KWFC	g	57046.75	2015-01-24	> 21.53
Kiso	KWFC	g	57047.77	2015-01-25	> 20.64
Kiso	KWFC	g	57049.70	2015-01-27	> 21.45
Akeno	MITSuME	g	57050.69	2015-01-28	> 20.85
Kiso	KWFC	g	57055.72	2015-02-02	> 20.26
Akeno	MITSuME	g	57062.54	2015-02-09	> 20.43
Akeno	MITSuME	g	57063.67	2015-02-10	> 20.45
OAO	MITSuME	g	57063.76	2015-02-10	> 19.19
OAO	MITSuME	g	57064.61	2015-02-11	> 20.20
Akeno	MITSuME	g	57064.74	2015-02-11	> 20.59
Kiso	KWFC	g	57064.74	2015-02-11	> 20.91
Kiso	KWFC	g	57073.63	2015-02-20	> 21.74
OAO188	KOOLS	g	57102.49	2015-03-21	19.82 ± 0.14
OAO188	KOOLS	g	57103.46	2015-03-22	18.70 ± 0.11
OAO188	KOOLS	g	57103.56	2015-03-22	18.58 ± 0.11
OAO188	KOOLS	g	57103.72	2015-03-22	18.94 ± 0.10
OAO188	KOOLS	g	57104.56	2015-03-23	19.45 ± 0.12
OAO	MITSuME	g	57106.64	2015-03-25	> 20.61
OAO	MITSuME	g	57129.59	2015-04-17	> 20.90
OAO	MITSuME	g	57133.60	2015-04-21	> 21.04
OAO	MITSuME	g	57166.57	2015-05-24	> 20.59
Subaru	HSC	g	57167.50	2015-05-25	21.74 ± 0.13
OAO	MITSuME	g	57167.53	2015-05-25	> 19.49
OAO	MITSuME	g	57174.49	2015-06-01	> 19.14
OAO	MITSuME	g	57176.54	2015-06-03	> 20.18
Kottamia	-	V	56726.93	2014-03-10	19.17 ± 0.13
Saitama	-	V	57063.54	2015-02-10	> 18.92
Kanata	HONIR	R_C	56712.62	2014-02-24	20.48 ± 0.16
Akeno	MITSuME	R_C	56726.51	2014-03-10	19.48 ± 0.21
Kanata	HONIR	R_C	56726.75	2014-03-10	19.73 ± 0.12

Table 2. (Continued)

telescope	instrument	filter	MJD	date (UT)	magnitude
Kottamia	-	R_C	56726.93	2014-03-10	20.01 ± 0.14
Akeno	MITSuME	R_C	56954.73	2014-10-24	> 19.56
Akeno	MITSuME	R_C	56955.73	2014-10-25	20.04 ± 0.19
Akeno	MITSuME	R_C	56957.73	2014-10-27	> 18.16
OAO	MITSuME	R_C	56957.80	2014-10-27	> 19.95
Akeno	MITSuME	R_C	56958.72	2014-10-28	20.24 ± 0.20
OAO	MITSuME	R_C	56958.80	2014-10-28	> 19.75
Murikabushi	MITSuME	R_C	56959.80	2014-10-29	20.35 ± 0.18
OAO	MITSuME	R_C	56959.84	2014-10-29	> 19.03
Murikabushi	MITSuME	R_C	56960.78	2014-10-30	20.51 ± 0.19
Murikabushi	MITSuME	R_C	56961.78	2014-10-31	20.73 ± 0.18
Akeno	MITSuME	R_C	56962.73	2014-11-01	> 19.97
Akeno	MITSuME	R_C	56963.71	2014-11-02	> 19.68
OAO	MITSuME	R_C	56963.83	2014-11-02	> 19.13
Akeno	MITSuME	R_C	56964.73	2014-11-03	> 20.14
OAO	MITSuME	R_C	56964.83	2014-11-03	> 19.65
Akeno	MITSuME	R_C	56965.75	2014-11-04	> 20.13
OAO	MITSuME	R_C	56965.83	2014-11-04	> 19.69
Akeno	MITSuME	R_C	56967.74	2014-11-06	> 19.94
OAO	MITSuME	R_C	56967.85	2014-11-06	> 18.32
Akeno	MITSuME	R_C	56968.78	2014-11-07	> 19.60
OAO	MITSuME	R_C	56971.83	2014-11-10	> 19.11
Akeno	MITSuME	R_C	56973.70	2014-11-12	> 19.89
Akeno	MITSuME	R_C	56974.69	2014-11-13	> 20.37
Akeno	MITSuME	R_C	56975.68	2014-11-14	> 19.91
Akeno	MITSuME	R_C	56976.68	2014-11-15	20.14 ± 0.19
Kanata	HONIR	R_C	56976.87	2014-11-15	> 18.18
Kanata	HONIR	R_C	56976.87	2014-11-15	> 19.67
Akeno	MITSuME	R_C	56977.67	2014-11-16	19.58 ± 0.19
Akeno	MITSuME	R_C	56978.71	2014-11-17	> 20.03
Akeno	MITSuME	R_C	56979.66	2014-11-18	> 20.50
Akeno	MITSuME	R_C	56980.69	2014-11-19	> 19.45
Murikabushi	MITSuME	R_C	56980.72	2014-11-19	> 20.32
Akeno	MITSuME	R_C	56981.66	2014-11-20	> 20.15
Murikabushi	MITSuME	R_C	56981.73	2014-11-20	20.86 ± 0.18
Kanata	HONIR	R_C	56981.73	2014-11-20	21.01 ± 0.13
Murikabushi	MITSuME	R_C	56989.71	2014-11-28	> 20.04
Akeno	MITSuME	R_C	57050.69	2015-01-28	> 20.18
Akeno	MITSuME	R_C	57062.54	2015-02-09	> 19.79
Akeno	MITSuME	R_C	57063.67	2015-02-10	> 20.26
OAO	MITSuME	R_C	57063.76	2015-02-10	> 18.85
OAO	MITSuME	R_C	57064.61	2015-02-11	> 19.74
Akeno	MITSuME	R_C	57064.74	2015-02-11	> 20.24
OAO188	KOOLS	R_C	57102.50	2015-03-21	19.27 ± 0.12
OAO188	KOOLS	R_C	57102.67	2015-03-21	18.95 ± 0.11
OAO188	KOOLS	R_C	57102.80	2015-03-21	18.62 ± 0.11
OAO188	KOOLS	R_C	57103.48	2015-03-22	18.13 ± 0.10
OAO188	KOOLS	R_C	57103.58	2015-03-22	18.07 ± 0.10
OAO	MITSuME	R_C	57106.64	2015-03-25	20.35 ± 0.20

Table 2. (Continued)

telescope	instrument	filter	MJD	date (UT)	magnitude
Kanata	HONIR	R_C	57106.66	2015-03-25	20.64 ± 0.12
OAO	MITSuME	R_C	57129.59	2015-04-17	19.48 ± 0.18
Akeno	MITSuME	R_C	57130.66	2015-04-18	> 20.07
OAO	MITSuME	R_C	57133.60	2015-04-21	19.98 ± 0.17
OAO	MITSuME	R_C	57166.57	2015-05-24	> 19.98
OAO	MITSuME	R_C	57167.53	2015-05-25	> 19.13
OAO	MITSuME	R_C	57174.49	2015-06-01	> 18.88
OAO	MITSuME	R_C	57176.54	2015-06-03	> 19.87
Subaru	FOCAS	i	56712.63	2014-02-24	20.72 ± 0.10
Kanata	HONIR	I_C	56726.77	2014-03-10	19.41 ± 0.14
Kottamia	-	I_C	56732.53	2014-03-16	18.91 ± 0.21
Akeno	MITSuME	I_C	56954.73	2014-10-24	> 18.85
Akeno	MITSuME	I_C	56955.73	2014-10-25	> 19.68
Akeno	MITSuME	I_C	56957.73	2014-10-27	> 17.19
OAO	MITSuME	I_C	56957.80	2014-10-27	> 19.37
Akeno	MITSuME	I_C	56958.72	2014-10-28	> 19.64
OAO	MITSuME	I_C	56958.80	2014-10-28	> 19.29
Murikabushi	MITSuME	I_C	56959.80	2014-10-29	19.99 ± 0.19
OAO	MITSuME	I_C	56959.84	2014-10-29	> 18.32
Murikabushi	MITSuME	I_C	56960.78	2014-10-30	20.08 ± 0.19
Murikabushi	MITSuME	I_C	56961.78	2014-10-31	> 19.56
Akeno	MITSuME	I_C	56962.73	2014-11-01	> 19.51
Akeno	MITSuME	I_C	56963.71	2014-11-02	> 19.11
OAO	MITSuME	I_C	56963.83	2014-11-02	> 18.43
Akeno	MITSuME	I_C	56964.71	2014-11-03	> 19.65
OAO	MITSuME	I_C	56964.83	2014-11-03	> 19.21
Akeno	MITSuME	I_C	56965.72	2014-11-04	> 19.68
OAO	MITSuME	I_C	56965.83	2014-11-04	> 19.19
Akeno	MITSuME	I_C	56967.72	2014-11-06	> 19.55
OAO	MITSuME	I_C	56967.85	2014-11-06	> 17.92
Akeno	MITSuME	I_C	56968.77	2014-11-07	> 19.19
OAO	MITSuME	I_C	56971.83	2014-11-10	> 18.80
Akeno	MITSuME	I_C	56973.70	2014-11-12	> 19.27
Akeno	MITSuME	I_C	56974.69	2014-11-13	> 19.75
Akeno	MITSuME	I_C	56975.68	2014-11-14	> 19.61
Akeno	MITSuME	I_C	56976.68	2014-11-15	> 19.76
Akeno	MITSuME	I_C	56977.67	2014-11-16	> 19.65
Akeno	MITSuME	I_C	56978.71	2014-11-17	> 19.61
Akeno	MITSuME	I_C	56979.66	2014-11-18	> 19.88
Akeno	MITSuME	I_C	56980.69	2014-11-19	> 18.84
Murikabushi	MITSuME	I_C	56980.72	2014-11-19	> 19.94
Akeno	MITSuME	I_C	56981.66	2014-11-20	> 19.63
Murikabushi	MITSuME	I_C	56981.73	2014-11-20	> 20.70
Murikabushi	MITSuME	I_C	56989.71	2014-11-28	> 19.02
Akeno	MITSuME	I_C	57050.65	2015-01-28	> 19.78
Akeno	MITSuME	I_C	57062.54	2015-02-09	> 18.27
Akeno	MITSuME	I_C	57063.67	2015-02-10	> 19.73
OAO	MITSuME	I_C	57063.76	2015-02-10	> 18.36
OAO	MITSuME	I_C	57064.61	2015-02-11	> 18.83

Table 2. (Continued)

telescope	instrument	filter	MJD	date (UT)	magnitude
Akeno	MITSuME	I_C	57064.74	2015-02-11	> 19.69
OAO188	KOOLS	I_C	57102.49	2015-03-21	19.07 ± 0.12
OAO188	KOOLS	I_C	57102.66	2015-03-21	18.86 ± 0.11
OAO188	KOOLS	I_C	57102.79	2015-03-21	18.53 ± 0.11
OAO188	KOOLS	I_C	57103.47	2015-03-22	18.28 ± 0.11
OAO188	KOOLS	I_C	57103.57	2015-03-22	17.92 ± 0.10
OAO	MITSuME	I_C	57106.64	2015-03-25	> 19.79
OAO	MITSuME	I_C	57129.59	2015-04-17	> 19.60
Akeno	MITSuME	I_C	57130.66	2015-04-18	> 19.38
OAO	MITSuME	I_C	57133.60	2015-04-21	19.55 ± 0.21
OAO	MITSuME	I_C	57166.57	2015-05-24	> 19.44
OAO	MITSuME	I_C	57167.53	2015-05-25	> 18.72
OAO	MITSuME	I_C	57174.49	2015-06-01	> 18.45
OAO	MITSuME	I_C	57176.54	2015-06-03	> 19.57
Kiso	KWFC	z	56958.82	2014-10-28	> 19.78
Kiso	KWFC	z	56959.84	2014-10-29	> 19.70
Nayuta	LISS	z	56984.50	2014-11-23	19.51 ± 0.12
Subaru	HSC	z	56987.50	2014-11-26	20.57 ± 0.11
Kiso	KWFC	z	57064.76	2015-02-11	> 18.99
OAO188	KOOLS	z	57102.67	2015-03-21	18.79 ± 0.12
OAO188	KOOLS	z	57103.47	2015-03-22	17.96 ± 0.12
OAO188	KOOLS	z	57103.58	2015-03-22	17.78 ± 0.11
Kanata	HONIR	J	56732.68	2014-03-16	18.32 ± 0.21
Nayuta	NIC	J	56981.75	2014-11-20	20.23 ± 0.21
Nayuta	NIC	J	57104.53	2015-03-23	18.38 ± 0.20
Nayuta	NIC	J	57106.67	2015-03-25	19.85 ± 0.21
Nayuta	NIC	H	56955.80	2014-10-25	19.64 ± 0.21
Nayuta	NIC	H	56964.79	2014-11-03	19.60 ± 0.21
Nayuta	NIC	H	56965.77	2014-11-04	19.62 ± 0.21
Nayuta	NIC	H	56981.76	2014-11-20	20.01 ± 0.20
Nayuta	NIC	H	57104.53	2015-03-23	17.79 ± 0.20
Kanata	HONIR	K_s	56726.77	2014-03-10	17.85 ± 0.21
Kanata	HONIR	K_s	56732.70	2014-03-16	17.68 ± 0.22
Kagoshima	-	K_s	56954.77	2014-10-24	> 14.87
Nayuta	NIC	K_s	56955.80	2014-10-25	18.91 ± 0.21
OAO188	ISLE	K	56959.86	2014-10-29	19.02 ± 0.21
Nayuta	NIC	K_s	56964.79	2014-11-03	> 18.89
Kagoshima	-	K_s	56965.74	2014-11-04	> 16.85
Nayuta	NIC	K_s	56965.77	2014-11-04	19.49 ± 0.21
Kagoshima	-	K_s	56975.71	2014-11-14	> 15.85
Kanata	HONIR	K_s	56976.87	2014-11-15	> 16.75
Kagoshima	-	K_s	56981.71	2014-11-20	> 16.15
Kanata	HONIR	K_s	56981.72	2014-11-20	> 17.27
Nayuta	NIC	K_s	56981.76	2014-11-20	19.73 ± 0.21
OAO188	ISLE	K	56981.84	2014-11-20	19.11 ± 0.20
Nayuta	NIC	K_s	56982.86	2014-11-21	> 18.89
Kagoshima	-	K_s	56988.70	2014-11-27	> 14.47
Nayuta	NIC	K_s	57104.51	2015-03-23	17.45 ± 0.20
Kanata	HONIR	K_s	57106.66	2015-03-25	> 17.75

Table 2. (Continued)

telescope	instrument	filter	MJD	date (UT)	magnitude
Nayuta	NIC	K_s	57106.67	2015-03-25	19.22 ± 0.20